Pergamon

PII: S0191-8141(97)00093-X

Journal of Structural Geology, Vol. 20, No. 1, pp. 21 to 31, 1998

0191-8141/98 $19.00 + 0.00

Relative timing of calcite twinning strain and fold–thrust belt development; Hudson Valley fold–thrust belt, New York, U.S.A.

JOHN H. HARRIS and BEN A. VAN DER PLUIJM

Department of Geological Sciences, University of Michigan Ann Arbor, MI 48109 U.S.A.

(*Received* 4 *April* 1997; *accepted in revised form* 29 *September* 1997)

Abstract—Coarse-grained limestone samples were collected across the Hudson Valley Fold–Thrust Belt with the aim of determining the temporal and spatial relationship between calcite twinning strain and fold–thrust belt development. The majority of the samples have well defined oblate strain ellipsoids with the maximum shortening axes (e_3) perpendicular to bedding strike, and e_3 magnitudes that range from ~1.5% to 6.5%. Whereas twinning magnitude does not vary systematically through the fold–thrust belt, twinning fabrics fall into two populations based on the presence of outcrop-scale deformational features. Calcite twinning strain preserved in samples from limestone layers absent of any small-scale penetrative deformation, such as cleavage and/or microfaults, are defined as component **A** strains. Component **A** strains generally have maximum shortening axes (e_3) inclined consistently less than, but in the same E–W direction as, bedding dip. The second population of calcite twinning strain, population **B**, occurs in limestones pervasively cut by cleavage and/or microfaults. Component **B** strains has maximum shortening axes (e_3) that are horizontal irrespective of bedding dip. Strain population **A** initiated as a pre-folding, layer-parallel shortening strain that was subsequently modified to its present orientation by active grain-scale rotation during flexural folding. Strain population **B** reflects post-folding superimposed homogeneous strain, and is restricted to limestone samples with relatively high clay content. © 1998 Elsevier Science Ltd.

INTRODUCTION

Since it was recognized that the calcite strain-gauge technique can be used to accurately measure the orientation and magnitude of small strains in carbonates (e.g. Friedman *et al.*, 1976; Groshong *et al.*, 1984a), it has been used to provide strain data from naturally and experimentally deformed limestones. The technique has been particularly useful in studying the kinematic evolution of fold–thrust belts, such as the Appalachians (e.g. Engelder, 1979b; Wiltschko *et al.*, 1985; Kilsdonk and Wiltschko, 1988), the Rocky Mountains (e.g. Craddock *et al.*, 1988) and the Helvetic Alps (e.g. Dietrich and Song, 1984; Groshong *et al.*, 1984a; Dietrich, 1986; Ferrill and Groshong, 1993a,b).

Foreland fold–thrust belts appear to develop through several stages of deformation characterized by distinct strain styles. First, layer-parallel shortening occurs before and/or coincident with initial folding and thrusting. Second, as thrusts begin to negotiate ramps, non-layer-parallel shortening, bending and interlayer slip are imposed on the rocks. Continued thrust transport will impose both pure and simple shear on the rocks. Finally, when the thrust system locks due to frictional coupling between footwall and hangingwall, strain affects the rocks as homogeneous bulk shortening (Wiltschko *et al.*, 1985; Evans and Dunne, 1991). The long-standing problem with the use of the calcite strain-gauge technique has been in the understanding of when, during the above stages, calcite twinning strains accumulate.

Several interpretations of the temporal relationship between calcite twinning strain and fold–thrust belt formation have been proposed. Most commonly, mechanical twinning of calcite is thought to occur during layer-parallel shortening, before the development of folds and faults (Spang and Groshong, 1981; Wiltschko *et al.*, 1985; Craddock and van der Pluijm, 1989; Ferrill and Groshong, 1993a). Because calcite strain-hardens after twinning, it is generally assumed that calcite twinning only records early strains and becomes resistant to subsequent strain during later fold–thrust belt development, unless the orientation of the strain changes dramatically (Wiltschko *et al.*, 1985; Kilsdonk and Wiltschko, 1988). If this is true, the calcite twinning strain gauge records strains related to the first stage in the development of fold–thrust belts, but does not measure strains related to the subsequent stages. Results from studies of calcite twinning strain in single structures in particular supports the hypothesis that calcite twinning records strain during layer-parallel shortening (Spang and Groshong, 1981; Kilsdonk and Wiltschko, 1988). Generally these studies have shown that the maximum shortening axes (e_3) lie in the plane of bedding and at a high angle to strike. These studies conclude that twinning strain imposed before folding is passively rotated with bedding to a present-day inclination (roughly equal to the dip of bedding). Laboratory experiments, showing calcite's resistance to twinning after the first in a series of multi-stage deformations, further support the idea that a calcite grain strain-hardens and that late strains are not recorded (Donath and Fruth, 1971; also see Teufel, 1980).

However, other workers have suggested that calcite twinning strains are imposed during later stages of fold–thrust development. Rowe and Rutter (1990) suggested that calcite twinning recorded strain related to nappe

emplacement in limestone layers proximal to thrust faults in the Cantabrian zone of northern Spain. Groshong *et al.* (1984a) attributed calcite twinning strains to late stage fold tightening. Other work reported by Compton (1966), Dieterich and Carter (1969) and Ferrill and Groshong (1993b) suggested that calcite continues to mechanically twin during the entire development of a fold. Using the geometric relationships between the orientations of maximum shortening and bedding dip, Dieterich and Carter (1969) argued that early, layer-parallel shortening strains were overprinted by later syn-folding strains, such that the strain ellipsoid derived from calcite twinning analyses represents the cumulative strain of the folded layer. The two main goals of this study are: (1) to deduce at which stage(s) in the development of the Hudson Valley Fold–Thrust Belt (HVB) calcite twinning strains accumulated and (2) to interpret the variation of calcite twinning strain across the HVB, using relationships with lithologic composition and mesoscopic structures.

GEOLOGICAL SETTING

Stratigraphically above the late Ordovician Taconic angular unconformity, the Hudson Valley Fold–Thrust Belt (HVB) represents thin-skinned deformation of Upper Silurian through Lower Middle Devonian strata of southeastern New York (Fig. 1). Although HVB deformation is a result of Appalachian plate interactions, the exact timing of deformation remains debated (Geiser and Engelder, 1983; Marshak and Engelder, 1987; Schimmrich, personal communication, 1996). Outcrops analyzed in this study are located along the east–west trending Rt. 23 in Catskill, NY, at the western edge of the Hudson River Valley between the towns of Kingston and Albany. Strata involved in the deformation are composed primarily of Devonian shallow-water carbonates, locally known as the Helderberg Group (Marshak and Engelder, 1987). Of particular interest to this study are the Manlius, Coeymans, Kalkberg, New Scotland and Becraft limestone members, with 40 m in aggregate thickness and composed of alternating coarse grained, thinly layered (< 1 m) limestone and shale (Fig. 2a).

Most of the rocks exposed along New York 23 have undergone deformation under relatively low pressure and temperature conditions (Marshak and Engelder, 1985). Structures range from regional-scale folds (~ 50–125 m in amplitude) and thrusts, to zones of outcrop-scale pressure solution cleavage and small-scale folds and faults. Calcite slip lineations and bedding-plane slip

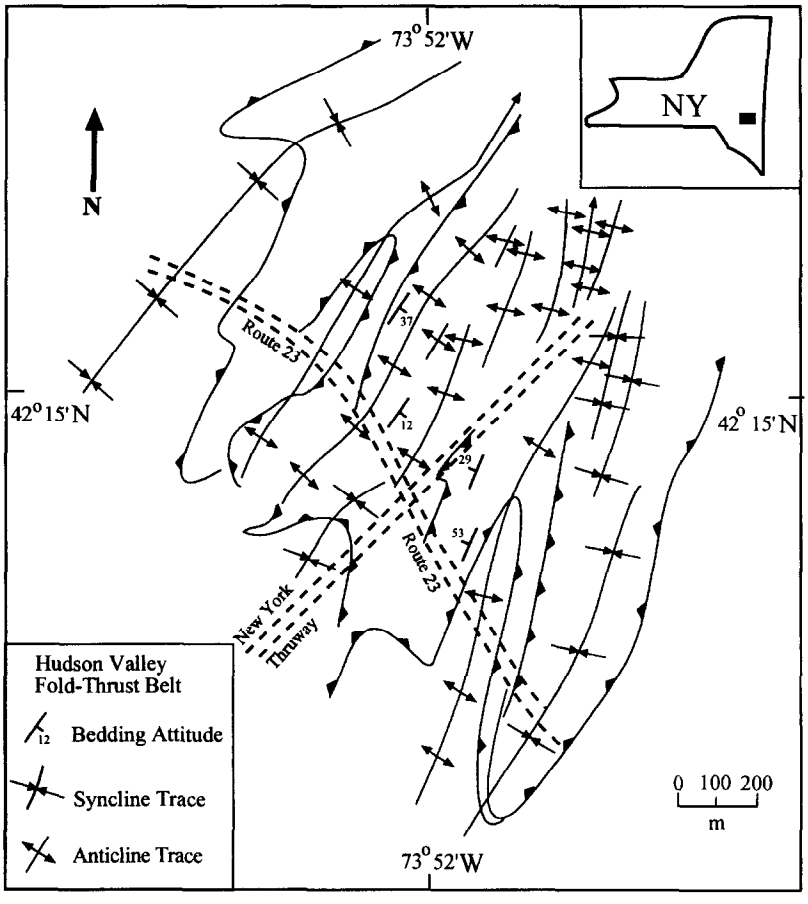

Fig. 1. Location of field area in New York State and generalized structure map of the Hudson Valley fold-thrust belt along New York Rt. 23 (after Marshak and Engelder, 1987).

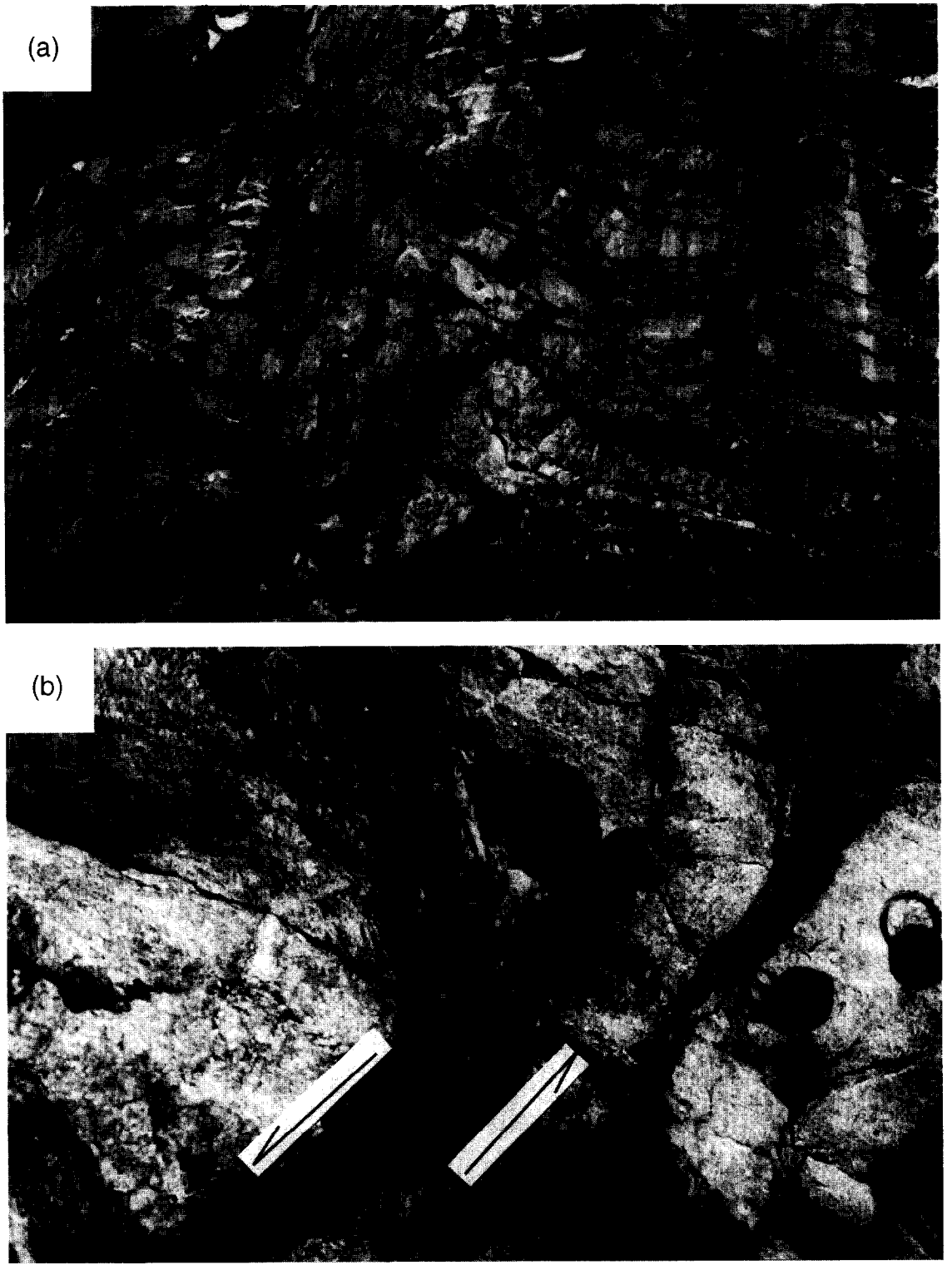

Fig. 2. Photograph of small scale fold (wavelength ~ 1.7 m) comprised of alternating limestone/shale layers exposed along Route 23 (a). Enlargement of the folded limestone/shale layers showing thickening of the shale layer in the hinge of the fold. Arrows indicate sense of shear affecting the folded layers (b).

surfaces indicate that flexural-slip was an important mechanism during folding. Cleavage intensity and minor folds in shale layers, commonly separating the limestone layers, suggest that considerable strain was accumulated in the less-competent shale layers (Fig. 2b). In zones of high strain, slip lineations, microfractures, microfaults, as well as cleavage, formed. Usually slip lineations and microfractures are spatially associated with faults within the more pure carbonate units, whereas cleavage domains occur in the more clay-rich units.

Striated veins cover fault surfaces and tend to propagate upward from fault planes to pervasively cross-cut mesoscopic structures. Studies of conodont coloration (Epstein *et al.*, 1977) and fission-track analysis (Lakatos and Miller, 1983) indicate that rocks of the HVB reached temperatures between 200 and 240°C, but it is not known if the time at which such temperatures were attained correlates with the time of deformation.

Cross-cutting relationships indicate that tectonic cleavage, more prevalent in clay-rich layers, developed early during the formation of the fold–thrust belt (Marshak and Engelder, 1985). Cleavage–fault intersection lineations are generally overprinted by calcite slip lineations that developed during fault movement. Early cleavage development is further supported by the observation that cleavage occurs in horizontal layers west of the study area along Rt. 23 (Engelder, 1979a). The field occurrence of such mesoscopic features will be used to determine calcite twinning strain populations.

SAMPLING AND METHODS

Samples were collected along a ~1 km section of outcrop exposed on Rt. 23 at a spacing of ~75–100 m. The aim of this sampling was to determine the variation in calcite twinning strain across the fold–thrust belt and, more specifically, to determine how twinning strains vary between and within structures on a regional scale. A second sample set was collected on a smaller scale (~1–5 m), concentrating on individual structures, with the aim of determining the relative timing between the formation of mesoscopic-scale structures and calcite twinning strain.

All 23 oriented samples were collected using a portable, gasoline-powered drill fitted with a 2.5 cm diameter diamond coring bit. Each sample was oriented with a compass using a standard paleomagnetic orientation device; structural measurements were made in the field using the same compass, with an estimated accuracy of 3°. By comparing twinning strains in drilled samples with twinning strains in hand samples we verified that sampling techniques were not responsible for twins in the samples. We used the calcite twinning strain technique (Groshong, 1972, Groshong *et al.*, 1984b) to calculate twinning strains in two or three mutually perpendicular thin sections from 22 of the 23 samples collected. Measurements were made using a Leitz (Ortholux II Pol-BK) polarizing microscope equipped with a five-axis Leitz Wetzlar universal stage. To process the optical data we used the CSG22 strain-gauge program described in Evans and Groshong (1994), which determines strain from all measurable twin sets within a population of calcite grains. As recommended by Groshong *et al.* (1984b), we removed the negative expected values (NEVs) that represent grains that were unfavorably oriented for twinning. Only four of the 20 analyzed samples have over 30% NEVs, and the removal of the NEVs from the remaining samples resulted in very small changes in strain orientations and magnitude. The nominal error of the strain magnitude is calculated as the average error of the normal strains in the x and y thin-section directions (Groshong *et al.*, 1984b).

STRAIN PATTERNS

Data from twinning strain analyses from across the study area are shown in a series of cross-sections (Fig. 3) and are listed in Table 1. The lower hemisphere, equal-area projections show the three principal strain axes and contours of the compression axes (Turner, 1953). In general, the principal shortening axes (e_3) are parallel to the maximum of contoured compression axes, and lie in an E–W plane that also contains the regional tectonic transport direction. The strain magnitude data, represented by e_3 (in percent shortening) do not appear to vary in a systematic fashion along the section. However, distinct strain geometries are recognized in samples with distinct field characteristics.

The strain data fall into two populations, from here on called components **A** and **B**, based on the existence of deformation structures in outcrop. Component **A** strain corresponds to rocks with no penetrative small-scale strain features such as microfaults and cleavage, whereas component **B** strain occurs in rocks collected in zones affected by cleavage and/or intense microfaulting. Component **A** strains have principal shortening axes (e_3) that plunge in the same direction but consistently less than bedding dip. The second strain population, component **B**, has principal shortening (e_3) axes which remain horizontal irrespective of bedding dip. These geometric relationships are shown in Fig. 4, which plots the bedding dip vs the plunge of e_3 for components **A** (Fig. 4a) and **B** (Fig. 4b), respectively (after Schwartz and Van der Voo, 1983).

DISCUSSION AND INTERPRETATION

The relationships between bedding dip and the principal shortening axes (e_3) shown in Fig. 4 may be used to explore, to a first-order, the relative timing of calcite twinning and deformation. If calcite twinning strains represent pre-folding, layer-parallel shortening strains, the inclination of the principal shortening axes (e_3) would be equal to the dip of bedding, and would fall along the diagonal in Fig. 4. This is not the case in either strain component **A** or **B**. In contrast, if calcite twinning represents post-folding strain, where the principal shortening axes (e_3) are imposed after the folds fully developed, the (e_3) axes would be horizontal irrespective of bedding dip, and would fall on a line parallel to the x-axis of the graphs in Fig. 4. Component **B** has this pattern, which is therefore interpreted as post-folding strain. Finally, if calcite twinning strains were acquired during

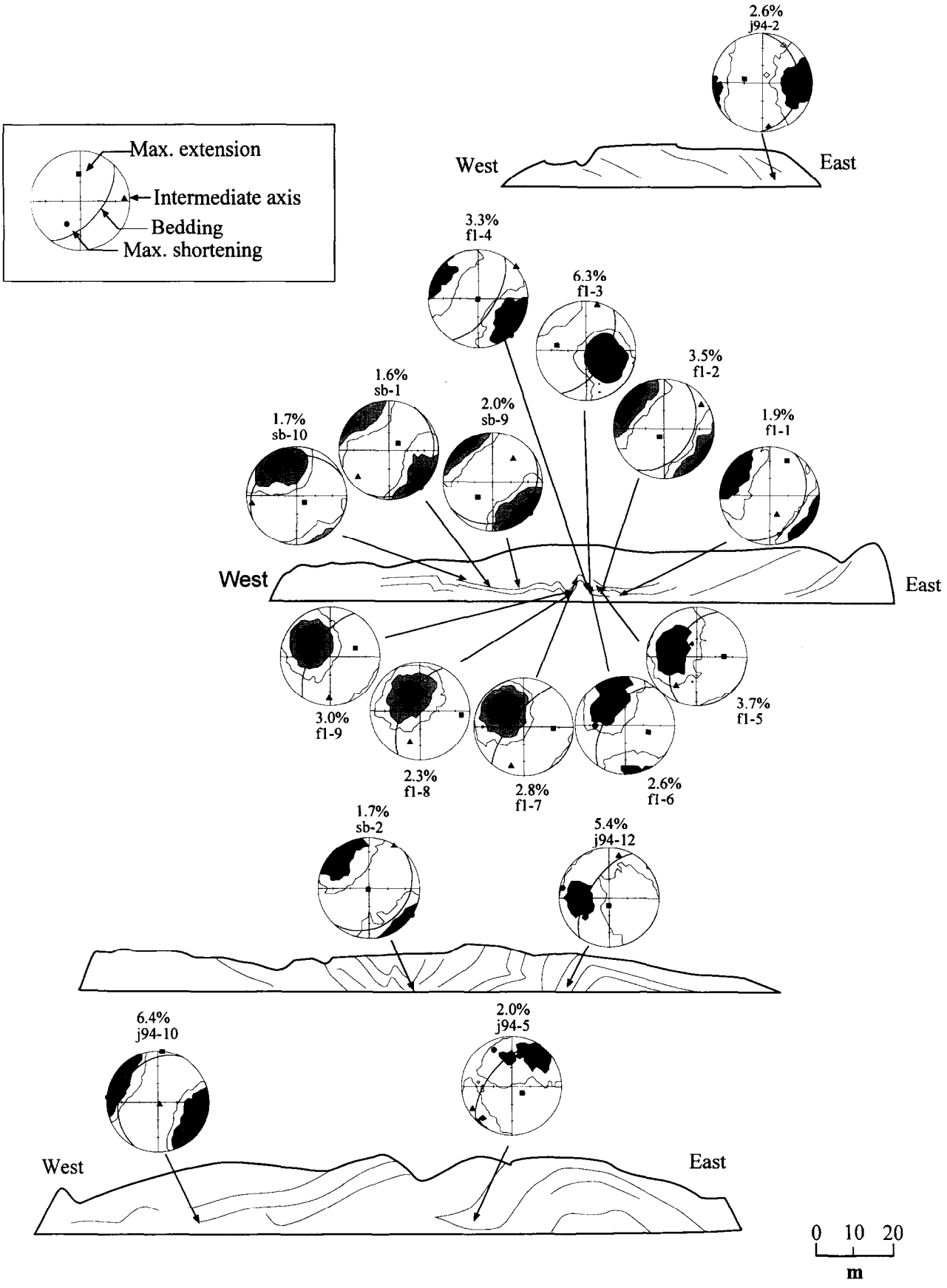

Fig. 3. Cross-sections showing variation in strain magnitude (% shortening), and equal-area lower hemisphere projections of strain axes and compression axes. The projections are oriented so that the top of the stereonets are oriented north. Compression axes contoured in multiples of standard deviation at 3σ and incremented by 2σ.

Table 1. Calcite strain data

Sample	All Data					Negative Expected Values Removed			
	e_1	e_2	e_3	% NEVs*	Error**	e_1	e_2	e_3	Error**
f1-1	1.90	0.73	−2.63	28	0.81	1.35	0.79	−2.14	0.44
f1-2	6.38	1.00	−7.38	17	1.62	3.05	0.83	−3.88	0.79
f1-2.2	3.50	1.51	−5.01	33	5.18	3.13	1.40	−4.54	1.90
f1-2.8	3.10	−0.36	−2.73	6	0.55	1.60	−0.23	−1.38	0.26
f1-3	7.73	2.22	−9.94	17	2.11	5.11	1.95	−7.06	0.83
f1-4	7.00	−1.93	−5.07	18	1.45	3.76	−1.80	−1.97	0.67
f1-5	3.17	0.09	−3.26	45	1.70	3.22	0.75	−3.98	1.03
f1-6	4.18	0.70	−4.87	17	1.73	2.54	0.18	−2.72	0.69
f1-7	4.73	1.38	−6.12	18	0.62	2.67	0.31	−2.89	0.32
f1-8	3.13	2.16	−5.29	6	0.80	1.55	1.12	−2.67	0.44
f1-9	4.85	1.21	−5.79	18	1.11	2.54	0.83	−3.37	0.56
j94-5	3.80	−0.87	−2.92	30	1.36	2.03	−0.16	−1.87	0.62
j94-10	6.89	6.07	−12.96	10	4.50	4.97	2.29	−7.27	3.02
j94-8	3.09	0.20	−3.29	24	1.29	2.25	0.43	−2.68	0.51
j94-12	6.26	1.54	−7.80	50	2.60	5.10	0.64	−5.74	2.98
j94-2	4.12	1.67	−5.80	0	0.49	2.06	0.84	−2.90	0.24
j-1	3.62	−1.32	−2.30	7	1.04	2.16	−0.77	−1.39	0.50
sb-1	3.21	0.15	−3.36	0	1.20	1.60	0.08	−1.68	0.60
sb-2	2.41	1.42	−3.83	8	1.03	1.26	0.70	−1.97	0.46
sb-4	2.05	−0.90	−1.15	58	2.04	3.78	−1.20	−2.58	0.66
sb-10	3.38	1.16	−4.54	13	1.20	1.15	0.81	−1.96	0.55
sb-9	2.86	1.19	−4.05	12	1.26	1.32	0.79	−2.11	0.53

*Percent of all twin sets having negative expected values for the shear strain calculated for that twin set.
**Standard error, $0.5\,(e_x + e_y) \times 10^2$; see Groshong *et al.* (1984).

folding then the data would, as is the case for strain component **A**, lie between the diagonal and the x-axis.

We have adopted the paleomagnetic fold test (Graham, 1949; McElhinny, 1964) to further explore the relationship between calcite twinning strain and folding. By adapting the statistical unfolding technique used by paleomagnetists to determine the relative timing of magnetization acquisition (McFadden and Jones, 1981), the timing of strain accumulation may be similarly quantified. The procedure is based on incrementally unfolding the inclined layers around the hinge line, while determining the clustering (e.g. the precision parameter **k**; Fisher, 1953) of the maximum shortening directions at each step. If the strain was acquired prior to folding the clustering of the shortening axes would be greatest when the bedding is restored to (paleo)horizontal. Conversely, if the strain was acquired after the bedding attitude was altered by tilting the clustering would become more scattered upon correction of the tilt.

The results from this 'fold test' show that the greatest clustering value, for component **A**, is achieved when the layer is ~75% unfolded (Fig. 5), suggesting that strain component **A** was acquired when the layers were ~25% folded. We further note that the principal shortening axes (e_3) at maximum clustering ($\mathbf{k}_{max}$) are horizontal, which is the orientation one expects for bulk horizontal shortening in fold–thrust belts. Component **B** strain, recorded in samples taken from locations proximal to cleavage and small-scale penetrative brittle deformation features, has **k** values that steadily decrease during stepwise unfolding, supporting our previous hypothesis that horizontal shortening strain was imposed after folding.

However, the folding model that is assumed in the above fold test may be overly simplistic. Therefore, by examining different deformation models for folding, we will test the potential for pre-folding, syn-folding and post-folding imposition of calcite twinning strains.

Passive vs active grain-scale rotation

Two end-member grain-scale deformation models during folding we explore are (1) the passive-rotation model (PRM) and (2) the active-rotation model (ARM). Passive rotation assumes that calcite twinning strains imposed under bulk horizontal shortening are subsequently rotated with the layer, but that no additional grain-scale rotation occurs. This model requires that after initial twinning the calcite grains strain-harden. Thus, if strain was imposed on the layered limestone either before or during the folding process, the principal strain axes will be passively rotated along with bedding. Implicit in this scenario is that, after strain accumulation, the principal shortening axes will maintain a constant angle with respect to bedding during subsequent folding.

Active grain rotation during flexural folding requires twinned calcite grains to be rotated by layer-parallel shear. Consequently, the orientation of the principal shortening axes (e_3) are rotated in a sense opposite to the direction of limb rotation. The angular rotation of particles is a function of: (1) the limb dip (i.e. the degree of angular shear) and (2) the physical coupling between particles. Ramsay (1967) calculates the angular rotation (b) as a function of dip angle (y) for constant area (Fig. 6a, b). Plotted as lines in Fig. 6c are limb rotation vs grain-scale rotation curves calculated for folds with full, half and quarter coupling, represented by Ω. Full coupling represents the theoretical maximum of grain-scale rotation in this model. Kodama (1988) suggested, based

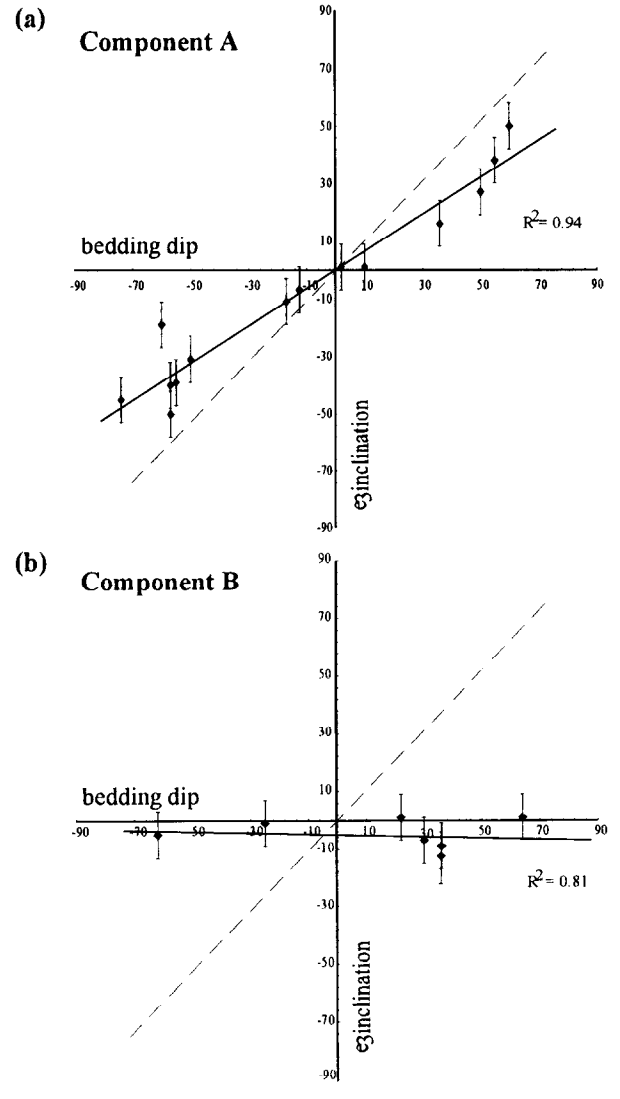

Fig. 4. Maximum shortening (e_3) axes vs bedding dip for strain component **A** (a) and component **B** (b). Dashed line represents values of equal bedding dip and e_3 axis-plunge. Error bars are $\pm 8°$ as calculated from Groshong *et al.* (1984b).

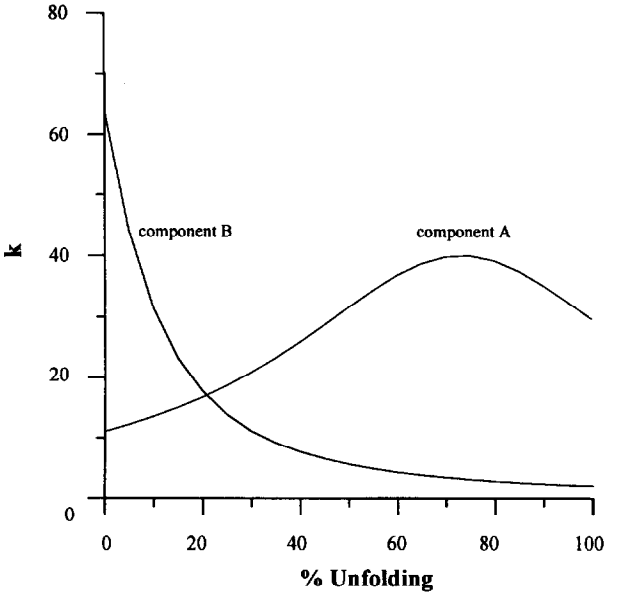

Fig. 5. Incremental fold tests showing variation in clustering parameter **k** as a function of percentage unfolding.

on the rotation of magnetizations in rocks of varying competency during deformation, that $\Omega < 0.3$ is a realistic coupling value for deformed Paleozoic carbonates in the Appalachian foreland.

Pre-folding twinning

If calcite twinning strains are imposed prior to folding, the strain orientations produced by subsequent folding will significantly vary depending on which folding mechanism is assumed. Depicted in Fig. 7a are the bedding dip and associated principal shortening (e_3) axes by both PRM and ARM. Under PRM, bedding dip and plunge of the principal shortening (e_3) axis would be equal at all stages of folding. Under ARM, the principal shortening (e_3) axis would plunge in the same direction, but at an angle consistently less than the dip of bedding. The magnitude of the angle between principal shortening (e_3) axis and layer dip is directly related to the degree of coupling between the grains.

Syn-folding twinning

If calcite twinning reflects syn-folding strain, the PRM and ARM models predict two different patterns. Assuming passive rotation during continued folding, the principal shortening (e_3) axes would always have a constant angle with bedding dip irrespective of the dip of bedding (Fig. 7b). If folding was accompanied by active grain rotation, the angle between the principal shortening (e_3) axes and layer dip would vary as a function of bedding dip, and the magnitude of the change would be directly related to the degree of grain-scale coupling. Within the same fold geometry, the magnitude of grain-scale rotation will be less for syn-folding ARM than pre-folding ARM.

Post-folding twinning

If twinning strains are imposed after folding is completed, there will, of course, be no later modification of the orientation of the principal shortening (e_3) axes. This implies that the principal shortening (e_3) axis, assuming only the superimposed homogenous strain model, will remain parallel to the horizontal bulk shortening direction (Fig. 7c).

ORIGIN OF STRAIN COMPONENTS A AND B

Although there is no unique test to determine which of these scenarios represents the correct interpretation for the two components of strain, we can define the likely

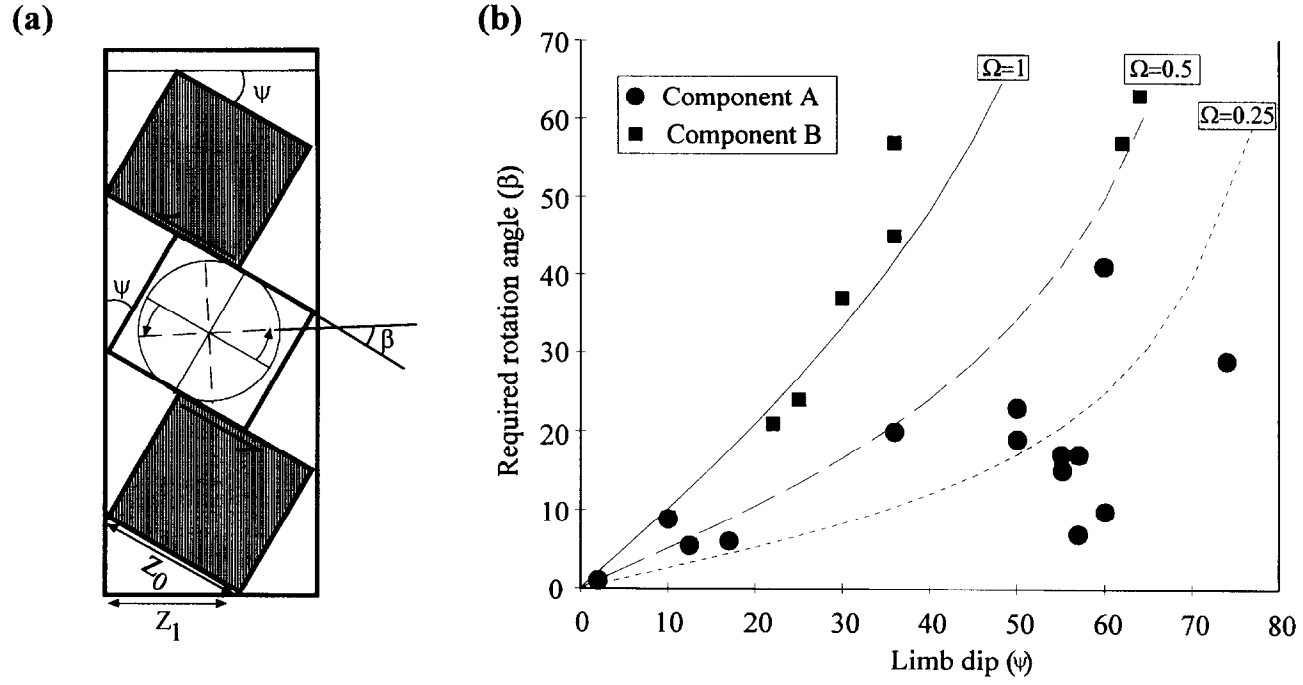

Fig. 6. Rigid-body rotation of particles during folding. In (a) the amount of rotation (β) as a function of limb dip (ψ) is illustrated; in (b), full, half and quarter coupling with constant area and $Z_1 = Z_0\cos\psi$ based on calculations in Ramsay (1967) are shown with measured rotations required for twinning strain components **A** and **B** superimposed.

scenario on the basis of what is most realistic within the structural environment of the study area and observations of calcite twinning patterns elsewhere. The models that are consistent with the occurrence of strain component **A** are: (1) pre-folding ARM, (2) syn-folding PRM, or (3) syn-folding ARM. Due to field evidence for the presence of flexural folding, we believe that active grain rotation was likely in some of the rocks during at least part of the folding process. Grain-scale rotations required for modeled pre-folding twinning strains are plotted as a function of limb rotation in Fig. 6b. Given the limb dips, the rotations required for strain component **A** represent coupling values that range from 0.2 to 0.35, which agree with other work on Paleozoic carbonates in eastern Pennsylvania (Kodama, 1988). Moreover, given the presence of calcite twins in unfolded strata of the Appalachian foreland immediately to the west (Craddock and van der Pluijm, 1989) we consider pre-folding twinning with active rotation as the most realistic scenario for component **A**.

Already we concluded that strain component **B** represents post-folding strain. Indeed, the required grain rotations as a function of limb rotation needed to explain component **B** yield unrealistically high coupling values that range from 0.75 to 1.25 (Fig. 6b). Syn-folding strain accumulation and passive rotation can also be dismissed because the principal shortening (e_3) axes are everywhere parallel to the horizontal bulk shortening direction. Component **B** strain, therefore, either reflects bulk homogeneous strain after the folds were locked (Fig. 7c), or syn-folding strain that has been modified to its present orientation. For the second scenario, the originally oblique shortening directions need to have been rotated into parallelism, and coincide with present-day horizontal. Such a condition is too fortuitous. Thus, we interpret strain component **B** as a post-folding, bulk homogeneous shortening.

During fold–thrust belt development, stress peaks may occur just before buckling and after fold tightening (Onasch, 1983). We argue that these two peaks correspond to the two twinning strain components observed in the HVB. If we accept this hypothesis there must be an explanation for why certain regions record twinning strains at different times. We suggest that the difference is related to the development of cleavage and other small-scale penetrative brittle strain in rocks of different mineralogy. We examined this by performing standard powder X-ray diffraction analyses on limestone samples which show that limestones with component **B** calcite twinning strains have larger clay content than those having component **A** strains.

To test for structural control on clay orientation in component **B** bearing limestone samples we used a single-crystal X-ray texture goniometer (see details in van der Pluijm *et al.*, 1994). This device collects X-ray intensity data as a thin rock sample ($\sim$200 μm thick) rotates relative to a narrow X-ray beam ($\sim$1 mm diameter). Figure 8 shows the orientation of illite and chlorite in limestone samples from the HVB, with component **B** strains showing parallelism with the cleavage orientation.

Marshak and Engelder (1985) also observed that limestone from the HVB with relatively high clay

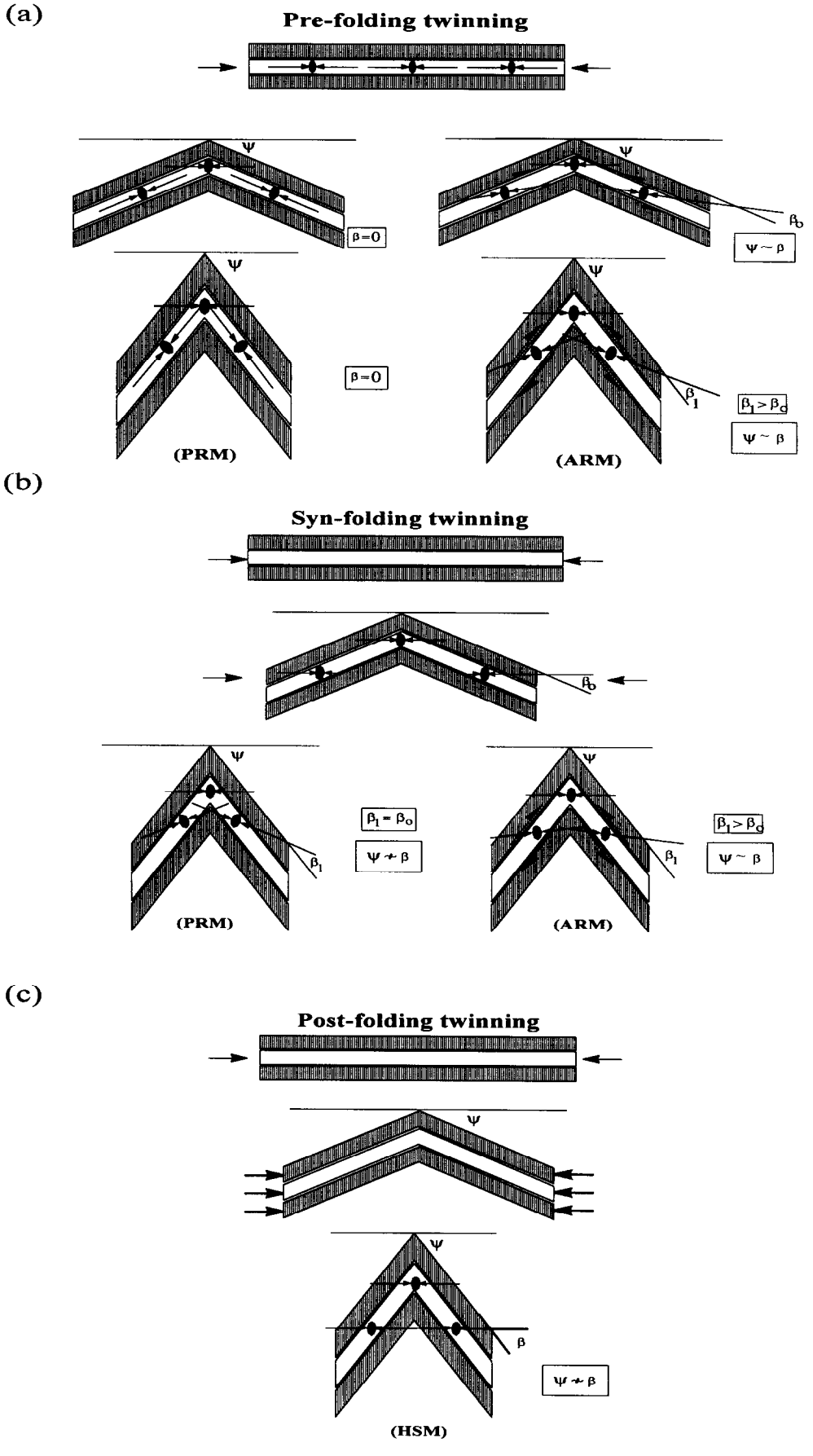

Fig. 7. Models of calcite twinning strain accumulation with respect to pre-folding (a), syn-folding (b) and post-folding (c), assuming both passive and active grain-scale rotation. See text for discussion.

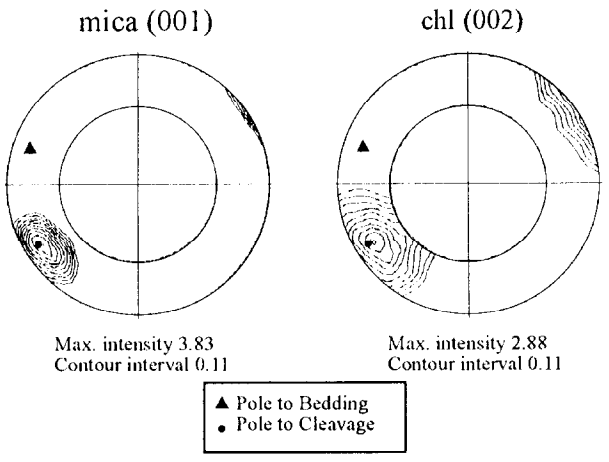

Fig. 8. Lower hemisphere equal-area projections of illite/mica (001) (left column) and chlorite (002) (right column) basal planes. Plots are contoured in multiples of random distribution (m.r.d.). Poles to bedding (triangles) and cleavage (circles) are labeled on each pole figure. Due to the angular limitations of the X-ray transmission mode, data are not recorded in the center of the projections.

contents (> 10%) were prone to cleavage development. From his work in the Appalachian Plateau, Engelder (1984) suggested that differential stresses of < 6.5 MPa are required for the initiation of cleavage, whereas differential stresses of < 20 MPa are required for calcite twinning (e.g. Wenk, 1985). Thus, clay-rich rocks, which are prone to early cleavage formation, will not reach stresses sufficiently high for twinning until cleavage can no longer develop. At this point the grain-scale stresses increase, allowing for calcite twinning to occur. In studies of quartz deformation lamellae in folded sandstone, Onasch (1983, also see Heald, 1956; Morris, 1981) presented similar conclusions. In pure quartzites and calcite-cemented sandstone, quartz deformation lamellae formed early without cleavage. In clayey sandstones however, cleavage formed early and deformation lamellae formed only after folds tightened.

CONCLUSIONS

Strain in the HVB, as deduced from the calcite strain-gauge technique, displays no obvious systematic variation in magnitude. However, the orientations of strain fall into two distinct populations. Strain component **A** is defined by an angular difference between layer dip and the principal shortening (e_3) axes that varies systematically as a function of bedding dip. Samples that contain strain component **A** come from areas with flexural folds that show no small-scale deformational features in outcrop. In contrast, samples containing strain component **B** occur in regions characterized by penetrative deformation features, including cleavage, microfaults and slip fractures. This component is defined by a horizontal principal shortening axis (e_3) irrespective of bedding dip. The presence of component **A** and **B** strains is directly related to mineralogic variations, in particular the clay content. We conclude that the two components of calcite twinning strain in the Hudson Valley Fold–Thrust Belt represent partitioning between pre-folding strain and superimposed homogeneous strain after folds in the belt locked up.

Acknowledgements—This work was supported in part by National Science Foundation grant EAR-9305736, and by grants from the Scott Turner Fund of the University of Michigan and the Geological Society of America. The computer program used for the calcite twinning strain analysis was written by Mark Evans and Richard Groshong. We thank Rob Van der Voo for commenting on an early version of the manuscript, John Stamatakos and Jay Busch for stimulating discussions and Steven Schimmrich, editor Jim Evans and an anonymous reviewer for constructive criticism.

REFERENCES

Alvarez, W., Engelder, T. and Lowrie, W. (1978) Formation of spaced cleavages and folds in brittle limestones by dissolution. *Geology* **4**, 689–701.

Compton, R. R. (1966) Analysis of Pliocene–Pleistocene deformation and stresses in northern Santa Lucia Range California. *Bulletin of Geological Society America* **77**, 1361–1380.

Craddock, J. P., Kopania, A. and Wiltschko, D. V. (1988) Interaction between the northern Idaho–Wyoming thrust belt and bounding basement blocks, central western Wyoming. *Memoirs of the Geological Society America* **171**, 333–351.

Craddock, J. P. and van der Pluijm, B. A. (1989) Late Paleozoic deformation of the cratonic carbonate cover of eastern North America. *Geology* **17**, 416–419.

Dieterich, J. H. and Carter, N. L. (1969) Stress-history of folding. *American Journal of Science* **267**, 129–154.

Dietrich, D. and Song, H. (1984) Calcite fabrics in a natural shear environment, the Helvetic nappes of western Switzerland. *Journal of Structural Geology* **6**, 19–23.

Dietrich, D. (1986) Calcite fabrics around folds as indicators of deformational history. *Journal of Structural Geology* **8**, 655–668.

Donath, F. A. and Fruth, L. S. (1971) Dependence of strain rate effects on deformation mechanism and rock type. *Journal of Geology* **79**, 347–371.

Engelder, T. (1979) Mechanisms for strain within the Upper Devonian clastic sequence of the Appalachian Plateau, western New York. *American Journal of Science* **279**, 527–542.

Engelder, T. (1979) The nature of deformation within the outer limits of the central Appalachian foreland fold and thrust belt in New York State. *Tectonophysics* **55**, 289–310.

Engelder, T. (1984) The role of pore water circulation during the deformation of foreland fold and thrust belts. *Journal of Geophysical Research* **89**, 4319–4325.

Epstein, A. G., Epstein, J. B. and Harris, L. D. (1977) Conodont color alteration—an index to organic metamorphism. Professional Paper, *United States Geological Survey* 995.

Evans, M. A. and Dunne, W. M. (1991) Strain factorization and partitioning in the North Mountain thrust sheet, central Appalachians U.S.A. *Journal of Structural Geology* **13**, 21–35.

Evans, M. A. and Groshong, R. H. (1994) A computer program for the calcite-strain technique. *Journal of Structural Geology* **16**, 277–282.

Ferrill, D. A. and Groshong, R. H. (1993) Deformation conditions in the northern Subalpine Chain, France, estimated from deformation modes in coarse-grained limestone. *Journal of Structural Geology* **15**, 995–1006.

Ferrill, D. A. and Groshong, R. H. (1993) Kinematic model for the curvature of the northern Subalpine Chain France. *Journal of Structural Geology* **15**, 523–541.

Fisher, R. A. (1953) Dispersion on a sphere. *Proceedings of the Royal Society of London, Series A* **217**, 295–305.

Friedman, M., Teufel, L. W. and Morse, J. D. (1976) Strain and stress analysis from calcite twin lamellae in experimental buckles and faulted drape folds. *Philosophical Transactions of the Royal Society of London, Series A* **283**, 87–107.

Geiser, P. A. and Engelder, T. (1983) The distribution of layer parallel shortening fabrics in the Appalachian foreland of New York and Pennsylvania: Evidence for two non-coaxial phases of the Alleghanian orogeny. *Memoirs of the Geological Society America* **158**, 161–175.

Graham, J. W. (1949) The stability and significance of magnetism in sedimentary rocks. *Journal of Geophysical Research* **54**, 131–167.

Groshong, R. H. (1972) Strain calculated from twinning in calcite. *Bulletin of Geological Society America* **83**, 2025–2038.

Groshong, R. H., Pfiffner, O. A. and Pringle, L. R. (1984a) Strain partitioning in the Helvetic thrust belt of eastern Switzerland from the leading edge to the internal zone. *Journal of Structural Geology* **6**, 5–18.

Groshong, R. H., Teufel, L. W. and Gasteiger, C. (1984b) Precision and accuracy of the calcite strain-gage technique. *Bulletin of the Geological Society America* **95**, 357–363.

Heald, M. T. (1956) Cementation of Simpson and St. Peter sandstones in parts of Oklahoma Arkansas and Missouri. *Journal of Geology* **64**, 16–30.

Kilsdonk, B. and Wiltschko, D. V. (1988) Deformation mechanisms in the southeastern ramp region of the Pine Mountain block Tennessee. *Bulletin of the Geological Society America* **100**, 653–664.

Kodama, K. P. (1988) Remanence rotation due to rock strain during folding and the stepwise application of the fold test. *Journal of Geophysical Research* **93**, 3357–3371.

Lakatos, S. and Miller, D. S. (1983) Fission-track analysis of apatite and zircon defines burial depth of 4–7 km for lowermost Upper Devonian Catskill Mountains, New York. *Geology* **11**, 103–104.

Marshak, S. and Engelder, T. (1985) Development of cleavage in limestones of a fold–thrust belt in eastern New York. *Journal of Structural Geology* **7**, 345–359.

Marshak, S. and Engelder, T. (1987) Exposures of the Hudson Valley Fold–Thrust Belt, west of Catskill, New York. in Roy, D. C. (ed.) Geological Society of America Centennial Field Guide (DNAG Series)—v.5, Northeastern Section, P. 123–128.

McElhinny, M. W. (1964) Statistical significance of the fold test in paleomagnetism. *Geophysics Journal of the Royal Astronomical Society* **8**, 240–338.

McFadden, P. L. and Jones, D. L. (1981) The fold test in palaeomagnetism. *Geophysics Journal of the Royal Astronomical Society* **67**, 53–58.

Morris, A. P. (1981) Competing deformation mechanisms and slaty cleavage in deformed quartzose meta-sediments. *Journal of Geological Society of London* **138**, 455–462.

Onasch, C. M. (1983) Dynamic analysis of rough cleavage in the Martisburg Formation, Maryland. *Journal of Structural Geology* **5**, 73–82.

Ramsay, J. G. (1967) *Folding and Fracturing of Rocks.* 568pp., McGraw-Hill.

Rowe, K. J. and Rutter, E. H. (1990) Paleostress estimation using calcite twinning: experimental calibration and application to nature. *Journal of Structural Geology* **12**, 1–17.

Schwartz, S. Y. and Van der Voo, R. (1983) Paleomagnetic evaluation of the orocline hypothesis in the Central and Southern Appalachians. *Geophysical Research Letters* **10**, 505–508.

Spang, J. H. and Groshong, R. H. (1981) Deformation mechanisms and strain history of a minor fold from the Appalachian Valley and Ridge Province. *Tectonophysics* **72**, 323–342.

Teufel, L. W. (1980) Strain analysis of experimental superposed deformation using calcite twin lamellae. *Tectonophysics* **65**, 291–309.

Turner, F. J. (1953) Nature and dynamic interpretation of deformation lamellae in calcite of three marbles. *American Journal of Science* **251**, 276–298.

van der Pluijm, B. A., Ho, N. C. and Peacor, D. R. (1994) High-resolution X-ray texture goniometry. *Journal of Structural Geology* **16**, 1029–1032.

Wenk, H. R. (1985) *Preferred Orientation in Deformed Metals and Rocks: An Introduction to Modern Texture Analysis.* Academic Press Inc., Orlando.

Wiltschko, D. V., Medwedeff, D. A. and Millson, H. E. (1985) Distribution and mechanisms of strain within rocks on the northwest ramp of the Pine Mountain Block, southern Appalachian foreland: A field test theory. *Bulletin of the Geological Society America* **96**, 426–435.